Title

Radiation-Induced Alterations in Synaptic Neurotransmission of Dentate Granule Cells Depend on the Dose and Species of Charged Particles

Journal

Radiation Research, 182(6)

ISSN

0033-7587

Authors

Marty, VN
Vlkolinsky, R
Minassian, N
et al.

Publication Date

2014-12-01

DOI

10.1667/rr13647.1

Peer reviewed

RADIATION RESEARCH **182**, 653–665 (2014)
0033-7587/14 $15.00

DOI: 10.1667/RR13647.1

Radiation-Induced Alterations in Synaptic Neurotransmission of Dentate Granule Cells Depend on the Dose and Species of Charged Particles

V. N. Marty,[a] R. Vlkolinsky,[b] N. Minassian,[a] T. Cohen,[a] G. A. Nelson[b] and I. Spigelman[a,1]

[a] *Division of Oral Biology and Medicine, UCLA School of Dentistry, University of California, Los Angeles, Los Angeles, California 90095; and*
[b] *Department of Basic Sciences, Division of Radiation Research, Loma Linda University, Loma Linda, California, 92354*

Marty, V. N., Vlkolinsky, R., Minassian, N., Cohen, T., Nelson, G. A. and Spigelman, I. Radiation-Induced Alterations in Synaptic Neurotransmission of Dentate Granule Neurons Depend on the Dose and Species of Charged Particles. *Radiat. Res.* 182, 653–665 (2014).

The evaluation of potential health risks associated with neuronal exposure to space radiation is critical for future long duration space travel. The purpose of this study was to evaluate and compare the effects of low-dose proton and high-energy charged particle (HZE) radiation on electrophysiological parameters of the granule cells in the dentate gyrus (DG) of the hippocampus and its associated functional consequences. We examined excitatory and inhibitory neurotransmission in DG granule cells (DGCs) in dorsal hippocampal slices from male C57BL/6 mice at 3 months after whole body irradiation with accelerated proton, silicon or iron particles. Multielectrode arrays were used to investigate evoked field synaptic potentials, an extracellular measurement of synaptic excitability in the perforant path to DG synaptic pathway. Whole-cell patch clamp recordings were used to measure miniature excitatory postsynaptic currents (mEPSCs) and miniature inhibitory postsynaptic currents (mIPSCs) in DGCs. Exposure to proton radiation increased synaptic excitability and produced dose-dependent decreases in amplitude and charge transfer of mIPSCs, without affecting the expression of γ-aminobutyric acid type A receptor α2, β3 and γ2 subunits determined by Western blotting. Exposure to silicon radiation had no significant effects on synaptic excitability, mEPSCs or mIPSCs of DGCs. Exposure to iron radiation had no effect on synaptic excitability and mIPSCs, but significantly increased mEPSC frequency at 1 Gy, without changes in mEPSC kinetics, suggesting a presynaptic mechanism. Overall, the data suggest that proton and HZE exposure results in radiation dose- and species-dependent long-lasting alterations in synaptic neurotransmission, which could cause radiation-induced impairment of hippocampal-dependent cognitive functions. © 2014 by Radiation Research Society

[1] Address for correspondence: UCLA School of Dentistry, Division of Oral Biology and Medicine, 10833 Le Conte Avenue, 63-078 CHS, Los Angeles, CA 90095-1668; e-mail: igor@ucla.edu.

INTRODUCTION

Exposure to protons and high-energy charged particle (HZE) radiation during long duration space travel represents a significant health risk for astronauts. Naturally occurring sources of space radiation include trapped radiation belts, galactic cosmic radiation (GCR), and solar particle events (SPE) that are composed of protons and nuclei of heavier elements such as iron and silicon. The traversal of such particles through biological matter is known to trigger intense ionization localized along their path, which is associated with generation of free radicals and clustered damage to macromolecules. Such radiation exposure is associated with oxidative stress to multiple cell types in various organs and tissues (*1–3*) including neurons in the hippocampus. Therefore, chronic exposure to GCR and SPE could have a detrimental impact on the well being and specifically on the neurophysiological status of astronauts during long-term space exploration (*4*). Exposure to such radiation can potentially induce a wide range of neurological consequences, and in animals it has been repeatedly shown to induce cognitive impairment (*1, 5, 6*). Although the mechanisms underlying this radiation-induced cognitive impairment are not clearly understood, previous studies suggest that the pathogenesis likely depends on multiple factors and may involve chronic oxidative stress (*7*), depletion of neuronal precursor cells of the hippocampus (*2, 8, 9*), neuroinflammation (*10, 11*), altered expression of the plasticity-related immediate early gene Arc (*6, 12, 13*) and impaired neurogenesis (*10, 14*). Indeed, it has been shown that exposure to iron radiation impairs the proliferation of hippocampal neural precursor cells in mice, and that the reductions in the generation of new neurons correlates in time with cognitive impairments seen in these mice (*10*).

The hippocampus plays an important role in normal brain function, including learning and memory. It receives major input from the entorhinal cortex through the perforant pathway to the dentate gyrus (DG) granule cells (DGCs). DGCs project through the mossy fiber pathway to the CA3 region pyramidal cells (*15*), which in turn project to the CA1 pyramidal cells through the Schaffer collaterals (*16*). The DG has attracted numerous studies because it is a site of active neurogenesis in the adult mammalian brain, which is

thought to contribute to the formation of new memories (*17–19*) and has been shown to be highly vulnerable to HZE-particle exposure (*20*). Moreover, pharmacological studies have demonstrated the importance of GABAergic and glutamatergic synaptic transmission of DGCs in maintaining cognitive health (*21–26*).

While it is well understood that radiation exposure induces impairments in hippocampal dependent cognitive performance (*1, 5, 6, 13*), little is known about the molecular mechanisms underlying these changes and whether they are associated with radiation-induced alterations in synaptic properties of DGCs. Due to different pattern of energy deposition and ionization track structures, irradiation with proton, silicon or iron may each have very different effects on cells and the overall neurological outcomes. Previous electrophysiological studies in the CA1 region of the hippocampus revealed that relatively high-dose (1–4 Gy) iron irradiation increases evoked synaptic potentials and decreases long-term plasticity (LTP) in mice (*27*). The purpose of this study was to determine the effects from exposure to low-dose proton, silicon and iron radiation on synaptic excitability of DGCs and to examine possible synaptic and/or cellular mechanisms that may cause these effects. We hypothesized that after examining radiation-induced changes in the synaptic excitability of DGCs with extracellular multielectrode array recordings, the mechanisms of such modifications could be further investigated at a single neuron level by recordings of pharmacologically isolated excitatory glutamatergic and inhibitory GABAergic synaptic currents. We tested this hypothesis 3 months postirradiation in hippocampal slices prepared from mice that were exposed to low-dose proton, silicon or iron radiation at ~3 months of age.

MATERIALS AND METHODS

Animals and Irradiation

The experiments described here were part of a program project involving five universities for which animal irradiations at Loma Linda University (LLU) and the Brookhaven National Laboratory (BNL) and associated logistics such as shipping were standardized to minimize environmental variations across the project, thus facilitating intercomparisons of measurements carried out by various expert teams. BNL scheduling and multi-user operations, limitations of postirradiation processing rates (one animal per day for electrophysiology), animal availability and other complex legislation-related factors were all factored into the study design. All animals were obtained from Jackson Laboratories, Bar Harbor, ME as approximately 9-week-old C57BL/6J males and housed at BNL for 1–2 weeks. Mice were irradiated at ages of 10–11 weeks old as part of BNL experimental campaign NSRL 11A (March/April, 2011) using silicon ions and campaign NSRL 11C (October/November, 2011) using iron ions. For postirradiation analyses, mice were shipped to LLU within 1 week after irradiation and then individually housed until later use. A subset of these animals was used for extracellular field recordings at LLU. The other subset was shipped to UCLA after approximately 75 days and used for patch clamp analysis within ~2 weeks of delivery to UCLA.

Animals were shipped directly from the vendor to LLU, where the mice were proton irradiated on a clinical beam line at the James M. Slater Proton Therapy and Research Center in March, July and December 2010. The animals used in the heavy-ion irradiation were also individually housed until later use. A subset of these animals was used for extracellular field recordings at LLU. The other subset was shipped to UCLA after approximately 75 days and used for patch clamp analysis ~2 weeks later. For all animals, electrophysiological recordings had to be conducted on several sequential days around the target date because of logistical constraints.

For radiation exposure, mice were loaded into $8 \times 3 \times 3$ cm plastic boxes with air holes and placed in a foam fixture in the beam line of the NASA Space Radiation Laboratory (NSRL). They were exposed to 600.5 MeV/nucleon $^{28}Si^{14+}$ ions or 594.7 MeV/nucleon $^{56}Fe^{26+}$ ions in a rectangular beam of approximately 20×20 cm with a useful central area of 18×18 cm over which intensity varied by $<5\%$. There was no modulation to the beam aside from beam line components and exposures therefore occurred in the plateau regions of the Bragg curve. The focused beam of HZE particles was generated by the Booster accelerator at BNL and transferred to the experimental beam line at the NSRL facility. Dose calibration was performed with three parallel plate ion chambers that were positioned upstream of target and a NIST-traceable Far West thimble chamber. The values of the thimble chamber were then compared with the upstream ion chambers so that the desired dose could be delivered to the samples based on upstream ion chamber measurements. The NSRL dosimetry system reported the LET for the silicon particles to be 43.6 keV/μm and the LET for the Fe particles to be 174.1 keV/μm.

The mice at LLU were loaded into the same restraint boxes and irradiated in the Bragg plateau region with a 20×20 cm circular beam of 150 MeV/nucleon protons (tuned energy) with a 1 cm plastic modulation and $<3\%$ variation in intensity across the central 18 cm. The beam energy at the target is reduced to ≈142 MeV/nucleon with a resulting LET of ≈0.57 keV/μm. The dosimetry was provided by the clinical control system calibrated to NIST-traceable ion chambers. Cohorts of mice were exposed to nominal doses of 0, 10, 50 and 100 cGy protons and 0, 25 and 100 cGy for Si and Fe. Sham-irradiated animals (0 cGy) were also loaded into the restraint boxes for 5 min and then returned to their cages. Actual doses received and post-irradiated tissue harvest times are summarized in Table 1.

Slice Preparation

Mice were euthanized at 90 ± 10 days after irradiation. Mice were anesthetized with 3.5% isoflurane (Phoenix, St. Joseph, MO) and decapitated. The brain was rapidly removed and immersed in ice-cold artificial cerebrospinal fluid (ACSF) containing: 125 m*M* NaCl, 2.5 m*M* KCl, 2 m*M* $CaCl_2$, 2 m*M* $MgCl_2$, 26 m*M* $NaHCO_3$ and 10 m*M* glucose, pH of 7.4 and saturated with 95% O_2/5% CO_2. Coronal brain slices (400 μm) containing the dorsal hippocampus were obtained with a vibrating slicer (Leica VT 1200S; Nussloch, Germany) from a block of tissue. Slices were allowed to recover for at least 1 h at room temperature.

Electrophysiology

Field excitatory postsynaptic potentials (fEPSPs) were recorded using a MED64 multi-electrode array (Panasonic, Japan). The MED64 multi-electrode was used in conjunction with a 16×4 channel divider (MED-B02; AlfaMED, Japan), thus evoked synaptic activity in 4 hippocampal slices could be measured simultaneously with 16 active electrodes per slice. Slices were gently transferred (one at a time) using a custom made plastic dropper on the 1% polyamine-coated multi-electrode MED64 chips (type P210A; AlfaMED, Japan). The slices were carefully positioned under visual guidance (low-magnification inverted microscope; Motic®, Speed Fair Co. Ltd., Hong Kong, China) above the active quadrant (16×4 electrode area) that usually

TABLE 1
Doses Received, Harvest Times Postirradiation and Cohort Sizes

	Protons		Silicon ions		Iron ions	
Use	Dose (cGy)	Postirradiation harvest dates (no. of mice)	Dose (cGy)	Postirradiation harvest dates (no. of mice)	Dose (cGy)	Postirradiation harvest dates (no. of mice)
Patch	0	93.5 ± 3.4	0	103.9 ± 7.4	0	100.7 ± 8.0
Clamp	10.05 ± 0.04	(11)	25.14 ± 0.07	(21)	25.08 ± 0.05	(24)
Recording	50.03 ± 0.03		100.19 ± 0.07		100.05 ± 0.01	
	100.60 ± 0.85					
MED 64	0	93.6 ± 3.8	0	101.9 ± 11.0	0	104.7 ± 12.1
Field	10.01 ± 0.02	(20)	25.17 ± 0.11	(26)	25.14 ± 0.10	(32)
Recording	50.00 ± 0.00		101.27 ± 2.19		100.09 ± 0.06	
	100.30 ± 0.56					

covered 80–90% of the dendritic region (*stratum moleculare*) in the enclosed blade of the dentate gyrus neuronal fields. Slices were covered with 0.7 × 0.7 cm synthetic mesh fabrics to prevent floating, then weighted down by gold-plated metal U-shaped anchor and visually inspected for proper electrode location. Incubation media was then removed momentarily to enhance slice adhesion on the chip surface and immediately replenished with 0.8 ml fresh prewarmed and oxygenated ACSF. A microphotograph of each slice was used for documentation and later offline analyses. Chips containing slices were transferred into MED C-03 electrode connector/chip holder. Perfusion caps (MED64, AlphaMED, Japan) were attached to each chip that allowed perfusions of prewarmed (in-line heater connected to TC-344 heat controller, Warner Instruments LLC, Hamden, CT), oxygenated ACSF (2 ml/min) and continuous humidified carbogen delivery (75 ml/min) to the slice microenvironment. Chips containing slices were maintained at 33.0 ± 0.2°C and continuously monitored by two independent thermistors TC-344 heat controllers. Each of the 16 electrodes (20 μm^2 electrode size, 100 μm inter-polar distance) could be used either for stimulation or for recordings. After careful morphological inspection of each slice, stimulation sites were carefully chosen in the anticipated path of axons of the medial perforant pathway (mPP). Thus, the stimulation sites were typically selected in the dendritic layer (*stratum moleculare*) of the granular cell located within one third of the enclosed blade of the DG, proximal to the sulcus. Such placement of the stimulation electrode typically evoked a well defined negative fEPSP recorded by the proximal recordings electrodes. While excitatory responses were detected by most of the electrodes, for quantitation we utilized responses originating from electrodes closest to the stimulation electrode (either 100 or 140 μm). Thus, the recording site was usually located between the stimulation electrode and the dentate granule cell layer (~50 μm from *stratum granulosum*). The mPP fibers were stimulated by delivering biphasic square current pulses of 0.2 ms duration at 0.05 Hz and compound fEPSPs were recorded in the DG. To ensure selective stimulation of the mPP, paired-pulse protocols were used (20–200 ms inter-pulse interval) to confirm paired-pulse inhibition of the second fEPSP in most recordings (data not shown).

Miniature postsynaptic currents were recorded using whole-cell patch clamp technique. Recordings were obtained from DGCs located in the upper blade of the DG cell layer at 34 ± 0.5°C during perfusion with ACSF. Borosilicate glass recording pipettes (TW150F-3, World Precision Instruments, Inc., Sarasota, FL) were pulled using an electrode puller (Model P-87; Sutter Instrument, Novato, CA) to 5–7 MΩ resistance. For inhibitory GABAergic synaptic transmission recordings, patch pipettes were filled with a solution containing: 127 m*M* CsCl, 2 m*M* $MgCl_2$, 1 m*M* $CaCl_2$, 11 m*M* EGTA, 3 m*M* K_2ATP, 0.3 m*M* Na_3GTP and 10 m*M* HEPES, pH adjusted to 7.3 with CsOH. For excitatory glutamatergic synaptic transmission recordings, patch pipettes were filled with a solution containing: 120 m*M* CsCl, 10 m*M* NaCl, 0.1 m*M* $CaCl_2$, 1 m*M* EGTA, 4 m*M* K_2ATP, 0.3 m*M* Na_3GTP and 10 m*M* HEPES, pH adjusted to 7.3 with CsOH. Once in whole-cell configuration, the cells were allowed to recover for at least 10 min before any experimental protocol was performed to allow equilibration and stabilization of ionic conductances. Access resistance (<30 MΩ) was monitored at the start and the end of the recordings. Recordings were accepted for analysis if access resistance changes were <20%. $GABA_A$R-mediated miniature inhibitory postsynaptic currents (mIPSCs) were pharmacologically isolated by adding 0.5 μ*M* tetrodotoxin (TTX), 40 μ*M* D-2-animo-5-phosphonopentanoate (APV), 10 μ*M* 6-cyano-7-nitroquinoxaline-2,3-dione (CNQX) and 1 μ*M* 5,7,8,9-tetrahydro-5-hydroxy-6*H*-benzocyclohepten-6-ylideneacetic acid hydrochloride (CGP54626) (Tocris Bioscience, Park Ellisville, MO) in ACSF. AMPAR-mediated miniature excitatory postsynaptic currents (mEPSCs) were pharmacologically isolated by adding 0.5 μ*M* TTX, 50 μ*M* picrotoxin (Ascent Scientific, Bristol, UK) and 1 μ*M* CGP54626 hydrochloride in ACSF. The mIPSCs and mEPSCs were recorded at a membrane holding potential of −70 mV. Electrophysiological signals were amplified using the Multiclamp 700B amplifier (Molecular Devices LLC, Union City, CA), low-pass filtered at 1 kHz and digitized at 10 kHz with the Digidata 1440A (Molecular Devices, Sunnyvale, CA).

Detection and Analysis of fEPSPs

The evoked fEPSP reflects the magnitude of postsynaptic dendritic depolarization in close vicinity around the recording electrode (*28*). The fEPSP peak-to-peak amplitude, maximal negative amplitude (minimal amplitudes) and initial linear fEPSP slope were measured and statistically evaluated. While all of these measurements reflect the magnitude of synaptic depolarization, they may slightly differ since they are further affected by temporal profile of the excitatory and inhibitory synaptic transients. Peak-to-peak analysis was used as the most robust measurement of fEPSP magnitude, while changes in fEPSP minimal amplitudes (data not shown) and initial linear slopes (data not shown) mostly followed the trends observed in the peak-to-peak analyses. Responses were evaluated by Mobius TM Window 7.0.3.9 Version (WitWerx Inc., AlphaMed, Osaka, Japan) online/offline built-in algorithms. Measurements were exported to Microsoft Excel for further data processing. Synaptic excitability was assessed in each individual slice with an input-output (I-O) test, using incrementally increasing stimulus intensities (5–150 μA). Incremental stimulation intensity (SI) recruited an increasing number of presynaptic terminals that resulted in a nearly linear increase of the dendritic fEPSP at this stimulation range. In most cases, the maximal stimulation intensity used in our experiments was below the threshold for induction of action potentials. Thus, synchronous neuronal firing of action potentials typically observed as population spikes was rarely present. If present, population spikes were observed at their threshold as a subtle distortion superimposed on fEPSP that did not confound the measurement of the fEPSP size (*27*).

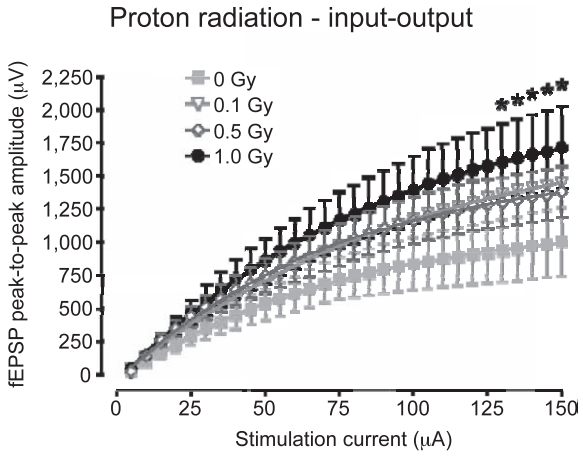

FIG. 1. Exposure to proton radiation increases synaptic excitability of DGCs. Summary graph of the input-output relationships illustrates significant increases in synaptic excitability of DGCs at 130–150 μA stimulation intensities (*$P < 0.05$, n = slices/mice: 0 Gy, n = 5/5; 0.1 Gy, n = 8/5; 0.5 Gy, n = 8/4; 1 Gy, n = 8/6) by a 1 Gy dose of proton radiation.

Detection and Analysis of mIPSCs and mEPSCs

Data were acquired using pCLAMP™ 10 software (Molecular Devices), and analyzed using Clampfit application software (Molecular Devices) and the Mini Analysis Program (Synaptosoft Inc., Decatur, GA). The recordings were low-pass filtered offline (Clampfit application software) at 2 kHz. The mIPSCs and mEPSCs were detected (Mini Analysis Program, Synaptosoft, Inc., Fort Lee, NJ) with threshold criteria of: amplitude, 5 pA and area, 20 fC. The mean frequency of mIPSCs and mEPSCs was determined for each cell as the number of events per second during a 100–300 s recording period. For kinetic analysis, only single event mIPSCs or mEPSCs with a stable baseline, sharp rising phase and exponential decay were chosen during visual inspection of the recording trace. Double and multiple peaks were excluded. The mIPSC and mEPSC kinetics were obtained from analysis of the averaged chosen single events aligned with half rise-time in each cell (100–300 events per cell). Decay time constants (τ1 and τ2) were obtained by fitting a double or single exponential to the falling phase of the averaged mIPSCs or mEPSCs, respectively. The synaptic charge transfer representing the magnitude of ion flow through $GABA_A$Rs or AMPARs was measured as the area under the best-fit curve of the average mIPSC or mEPSC, respectively.

Western Blot Analysis

Isolated hippocampus tissues were homogenized in ice-cold homogenate buffer containing: 124 m*M* NaCl, 3.2 m*M* KCl, 1.06 m*M* NaH_2PO_4, 2.5 m*M* $CaCl_2$, 1.3 m*M* $MgCl_2$, 26 m*M* $NaHCO_3$ and 10 m*M* glucose, bubbled with 95% O_2/5% CO_2 to adjust pH at 7.4. Protease inhibitors (1:20; P8340, Sigma-Aldrich LLC, St. Louis, MO) were included in the buffer to minimize proteolysis. The lysate was centrifuged for 15 min (14,000*g*, 4°C) and supernatants were collected for Western blot analysis. Protein concentrations were determined with BCA Protein Assay Kit (Pierce™, Rockford, IL) according to the manufacturer's instructions. Equal quantities of proteins (20 μg/lane) were electrophoretically separated on a 10% SDS-PAGE (Bio-Rad, Hercules, CA). Proteins were transferred to polyvinylidene fluoride (PVDF) membranes (Bio-Rad). After saturation in Tris-buffered saline (TBS) with 0.05% Tween™ 20 containing 5% nonfat dry milk (Bio-Rad), the PVDF membranes were probed with $GABA_A$ receptor ($GABA_A$R) α2 or with anti-$GABA_A$R β3 (clone N87/25, UC Davis/NIH NeuroMab Facility, Davis, CA), or with anti-$GABA_A$R γ2 at 1:1,000, or with rabbit polyclonal β-actin (AB8227, Abcam®, Cambridge, MA) at 1:2,000 and were incubated overnight at 4°C. W. Sieghart and colleagues (Medical University of Vienna, Vienna, Austria) kindly provided the α2 and γ2 $GABA_A$R subunit antibodies. After washing in TBS with 0.05% Tween 20, PVDF membranes were incubated with the corresponding peroxidase-conjugated secondary antibody for 1 h at room temperature. Gel bands were revealed by chemiluminescence (ECL, Pierce) and pictures were acquired with a camera system of luminescent image analyzer (LAS-3000, Fujifilm, Tokyo, Japan). Optical density analysis of the signals was performed using ImageJ64 software (ImageJ 1.43u, NIH). The integral of the entire optical density profile was calculated as the final value. β-actin was used as a loading control in all experiments.

Statistics

The investigators performing the recordings and analysis were blind to the treatment that the mice received. Data were expressed as mean ± standard error (SE). Statistical analyses were performed with one-way ANOVA or two-way repeated measures (RM) ANOVA followed by Bonferroni post hoc tests. A value of $P < 0.05$ was considered statistically significant.

RESULTS

Proton Radiation Increases Synaptic Excitability of DGCs

To determine the effect of low-dose proton irradiation on synaptic excitability at perforant pathway to DGCs, we performed an input-output (I-O) test and evaluated the size of field excitatory postsynaptic potentials (fEPSPs) (Fig. 1A). As expected, incremental stimulation intensity significantly increased the fEPSP peak-to-peak amplitude in all 4 experimental groups [$F(29,696) = 114.4$, ***$P < 0.001$, two-way RM ANOVA)]. Importantly, we observed an interaction between stimulation intensity and proton-radiation doses [$F(87,696) = 1.9$, ***$P < 0.001$, two-way RM ANOVA]. Post hoc analysis showed that 1 Gy proton irradiation significantly increases fEPSP peak-to-peak amplitude at the highest stimulation intensities (SI) (SI: 130 nA, 0 Gy; 937 ± 236 μV, n = 5 vs. 1 Gy; 1,792 ± 258 μV, n = 7, *$P < 0.05$; SI: 150 nA, 0 Gy; 1,000 ± 261 μV, n = 5 vs. 1 Gy; 1,916 ± 272 μV, n = 7; *$P < 0.05$, Bonferroni post hoc test). However, such effect was not statistically significant at the 0.1 and 0.5 Gy doses. These data suggest that the excitability of the DGCs is increased after a 1 Gy dose of proton radiation.

Proton Radiation Decreases GABAergic Synaptic Transmission in DGCs

The increased synaptic excitability of DGCs observed in proton-irradiated mice could be due to a decrease in inhibitory GABAergic synaptic transmission. To determine the effect of low-dose proton radiation on inhibitory synaptic transmission in DGCs, mIPSCs were recorded from DGCs of 0, 0.1, 0.5 and 1 Gy proton-irradiated mice. Proton irradiation produced significant dose-dependent decreases in the amplitude of mIPSCs (0 vs.1 Gy, *$P <$

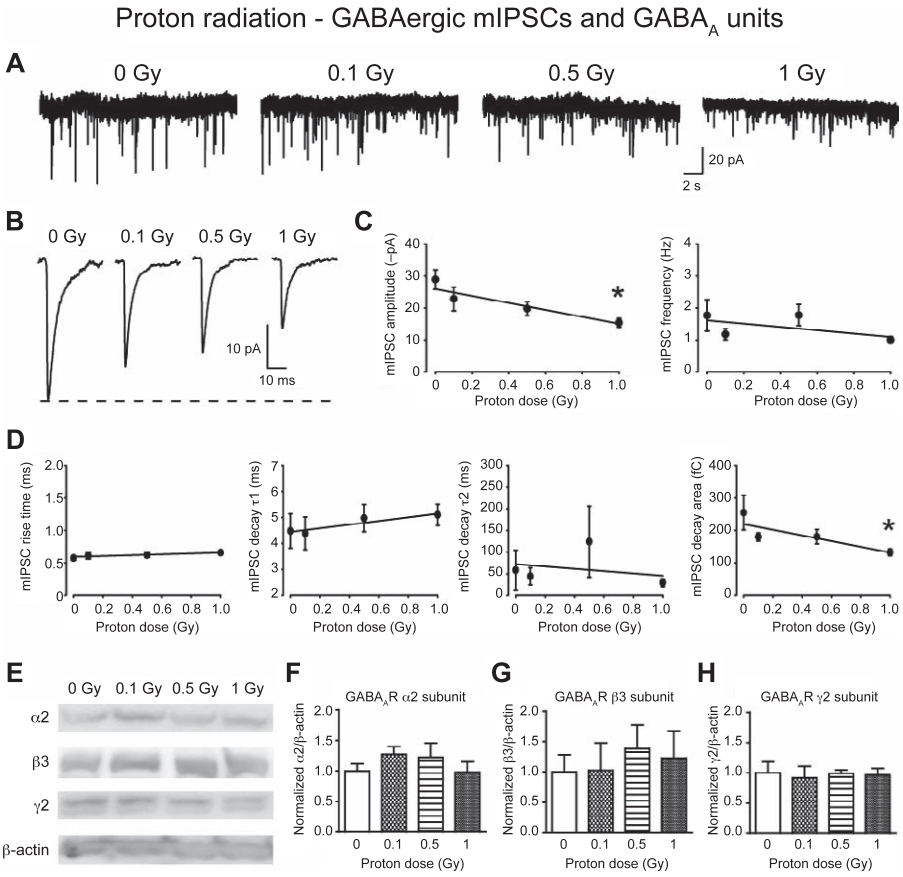

FIG. 2. Exposure of proton radiation decreases GABAergic synaptic transmission in the DG without affecting expression of $GABA_AR$ α2, β3 and γ2 subunits. Panel A: Representative current traces of miniature IPSCs recorded from DGCs of 0, 0.1, 0.5 and 1 Gy proton-irradiated mice. Panel B: Average mIPSC traces from representative DGCs of 0, 0.1, 0.5 and 1 Gy proton-irradiated mice. Panel C: Summary graphs showing the dose-dependent decrease in mIPSC amplitude in proton-irradiated mice (*$P < 0.05$, n = neurons/mice: 0 Gy, n = 6/4; 0.1 Gy, n = 7/3; 0.5 Gy, n = 7/4; 1 Gy, n = 13/2), while the frequency of mIPSCs was not affected. Panel D: Summary graphs showing that mIPSC rise time and decay time (τ1 and τ2 constant) are not affected by proton radiation, whereas mIPSC area under the curve is significantly decreased in 1 Gy proton-irradiated mice (*$P <$ 0.05). Panel E: Representative Western blots of $GABA_AR$ subunits α2, β3 and γ2 from the DG of 0, 0.1, 0.5 and 1 Gy proton-irradiated mice. β-actin was used as a loading control. Panels F–H: Summary graphs showing the lack of significant effect of proton radiation on the expression of $GABA_AR$ α2 (panel F), $GABA_AR$ β3 (panel G) and γ2 (panel H) subunits. Results are presented as a ratio with β-actin (n = 3 mice per subunit per radiation dose).

0.05, one-way ANOVA with Bonferroni posthoc test) but no changes in the frequency of mIPSCs ($P > 0.05$, one-way ANOVA) (Fig. 2A–C; Table 2). We also observed a significant decrease in mIPSC charge transfer in 1 Gy proton-irradiated mice (0 vs. 1 Gy, *$P < 0.05$, Kruskal-Wallis one-way ANOVA on ranks with Bonferroni post hoc test), but no changes in mIPSC rise time ($P > 0.05$, one-way ANOVA) and decay time (τ_1, $P > 0.05$, one-way ANOVA; τ_2, $P > 0.05$, Kruskal-Wallis one-way ANOVA on ranks) (Fig. 2D and Table 2). These results suggested that proton radiation reduces GABAergic synaptic transmission through postsynaptic mechanisms affecting $GABA_AR$ functional properties and/or expression. This decrease in inhibitory GABAergic synaptic transmission could represent the synaptic mechanism underlying the increased synaptic excitability of DGCs observed in extracellular recordings of fEPSPs from proton-irradiated mice.

Proton Radiation Does Not Modify the Expression of $GABA_AR$ α2, β3 and γ2 Subunits

The channel kinetics and pharmacological sensitivity of $GABA_ARs$ are largely dictated by their subunit composition and phosphorylation/dephosphorylation states (*29, 30*). Therefore, we examined if the proton radiation-induced decreases in postsynaptic $GABA_AR$ function could be mediated by alterations in the relative expression of individual $GABA_AR$ subunits. We focused on α2, β3 and γ2 subunits, because these are common subunits at DGC inhibitory synapses (*31, 32*). Immunoblotting analysis revealed no significant changes in the expression of $GABA_AR$ α2, β3 or γ2 subunits in irradiated mice compared

TABLE 2
Effects of Proton, Silicon and Iron Radiation on mIPSC Parameters

Patch clamp radiation (no. of DGCs recorded)	mIPSC					
	Amplitude (pA)	Frequency (Hz)	Rise time (ms)	Decay τ1 (ms)	Decay τ2 (ms)	Area (fC)
Proton						
0 Gy (6)	28.9 ± 3.1	1.8 ± 0.5	0.6 ± 0.03	4.5 ± 0.7	58.6 ± 45.8	255 ± 53
0.1 Gy (7)	22.8 ± 3.7	1.2 ± 0.2	0.6 ± 0.05	4.4 ± 0.6	44.4 ± 19.8	180 ± 13
0.5 Gy (7)	19.8 ± 2.1	1.8 ± 0.3	0.6 ± 0.04	5.0 ± 0.5	124.2 ± 82	181 ± 22
1 Gy (13)	15.4 ± 1.4[a]	1.0 ± 0.1	0.7 ± 0.02	5.1 ± 0.4	29.5 ± 9.0	133 ± 11[a]
Silicon						
0 Gy (16)	20.9 ± 1.9	3.2 ± 0.3	1.3 ± 0.4	4.0 ± 0.3	13.3 ± 2.1	310 ± 22
0.25 Gy (19)	24.4 ± 1.5	3.3 ± 0.2	0.8 ± 0.1	3.8 ± 0.2	11.9 ± 0.8	361 ± 18
1 Gy (19)	21.4 ± 1.6	3.2 ± 0.4	1.0 ± 0.2	4.2 ± 0.4	12.7 ± 2.1	344 ± 17
Iron						
0 Gy (15)	24.8 ± 1.7	1.9 ± 0.2	0.6 ± 0.02	4.8 ± 0.3	14.4 ± 1.8	324 ± 28
0.25 Gy (13)	29.4 ± 2.8	1.7 ± 0.3	0.6 ± 0.03	4.3 ± 0.3	12.9 ± 1.1	352 ± 31
1 Gy (14)	30.5 ± 2.8	1.6 ± 0.2	0.6 ± 0.03	4.3 ± 0.4	16.5 ± 3.3	319 ± 33

Note. 0 Gy vs. 1 Gy.
[a] $P < 0.05$, one-way ANOVA.

to nonirradiated mice ($GABA_AR$ α2/β-actin: 0 Gy: 100 ± 12%, n = 3 mice; 0.1 Gy: 127 ± 13%, n = 3 mice; 0.5 Gy: 122 ± 23%, n = 3 mice; 1 Gy: 98 ± 16%, n = 3 mice; $P > 0.05$, one-way ANOVA; $GABA_AR$ β3/β-actin: 0 Gy: 100 ± 28%, n = 3 mice; 0.1 Gy: 103 ± 45%, n = 3 mice; 0.5 Gy: 139 ± 39%, n = 3 mice; 1 Gy: 123 ± 44%, n = 3 mice; $P > 0.05$, one-way ANOVA; $GABA_AR$ γ2/β-actin: 0 Gy: 100 ± 18%, n = 3 mice; 0.1 Gy: 92 ± 19%, n = 3 mice; 0.5 Gy: 99 ± 6%, n = 3 mice; 1 Gy: 96 ± 10%, n = 3 mice; $P > 0.05$, one-way ANOVA) (Fig. 2E–H). These data suggested that proton radiation does not affect the expression of $GABA_AR$ subunits in the DG. Thus, one of the effects of proton radiation on GABAergic synaptic transmission may be due to modifications of phosphorylation/ dephosphorylation states of postsynaptic $GABA_AR$ function rather than changes in subunit expression.

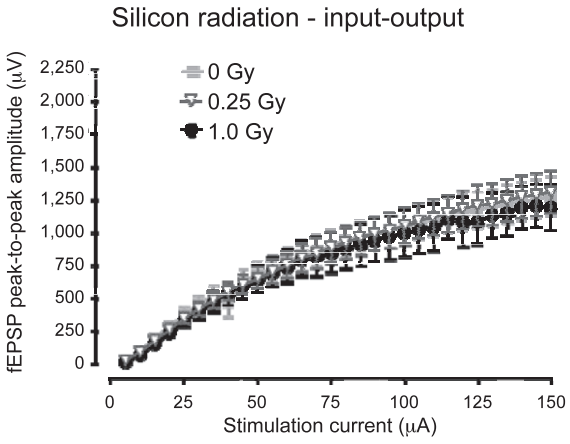

FIG. 3. Exposure to silicon radiation does not modify synaptic excitability in the DG. Summary of input-output relationship showing that exposure to silicon radiation does not modify the synaptic excitability of DGCs (n = slices/mice: 0 Gy, n = 17/12; 0.25 Gy, n = 13/11; 1 Gy, n = 16/11).

Silicon Radiation Does Not Affect Synaptic Excitability in DGCs

Recordings obtained from DGCs of silicon-irradiated mice were used to assess the effect of silicon radiation on DG synaptic transmission. The I-O tests of synaptic excitability in DGCs were not modified in mice irradiated with silicon compared to controls. As expected, increased stimulation intensity significantly increased fEPSP magnitude [$F(29,1237) = 141.2$, $^{***}P < 0.001$, two-way RM ANOVA]. However, silicon radiation did not significantly affect the I-O curves at any of the stimulation intensities [$F(2,1237) = 0.11$, $P > 0.05$, two-way RM ANOVA; stimulation intensity: 150 nA, fEPSP peak-to-peak amplitude: 0 Gy: 1272 ± 149 μV, n = 17; 0.25 Gy: 1304 ± 163 μV, n = 12; 1 Gy: 1187 ± 176 μV, n=15)] (Fig. 3A).

Silicon Radiation Does Not Affect GABAergic or Glutamatergic Synaptic Transmission in DGCs

Recordings of inhibitory GABAergic and excitatory glutamatergic synaptic transmission from DGCs of mice irradiated with 0.25 and 1 Gy of silicon were conducted under pharmacological isolation of mIPSCs (Fig. 4) or mEPSCs (Fig. 5). Silicon radiation had no effect on mIPSC amplitude ($P > 0.05$, one-way ANOVA) or frequency ($P > 0.05$, Kruskal-Wallis one-way ANOVA on ranks) in the DG (Fig. 4C and Table 2). No effect was observed on mIPSC rise time ($P > 0.05$, Kruskal-Wallis one-way ANOVA on ranks), decay time (τ_1, $P > 0.05$, Kruskal-Wallis one-way ANOVA on ranks; τ_2, $P > 0.05$, Kruskal-Wallis one-way ANOVA on ranks) and area under the curve ($P > 0.05$, one-way ANOVA) (Fig. 4D and Table 2).

Silicon radiation also had no effect on mEPSC amplitude ($P > 0.05$, Kruskal-Wallis one-way ANOVA on ranks) and frequency ($P > 0.05$, Kruskal-Wallis one-way ANOVA on ranks) (Fig. 5C and Table 3), nor on mEPSC rise time ($P >$

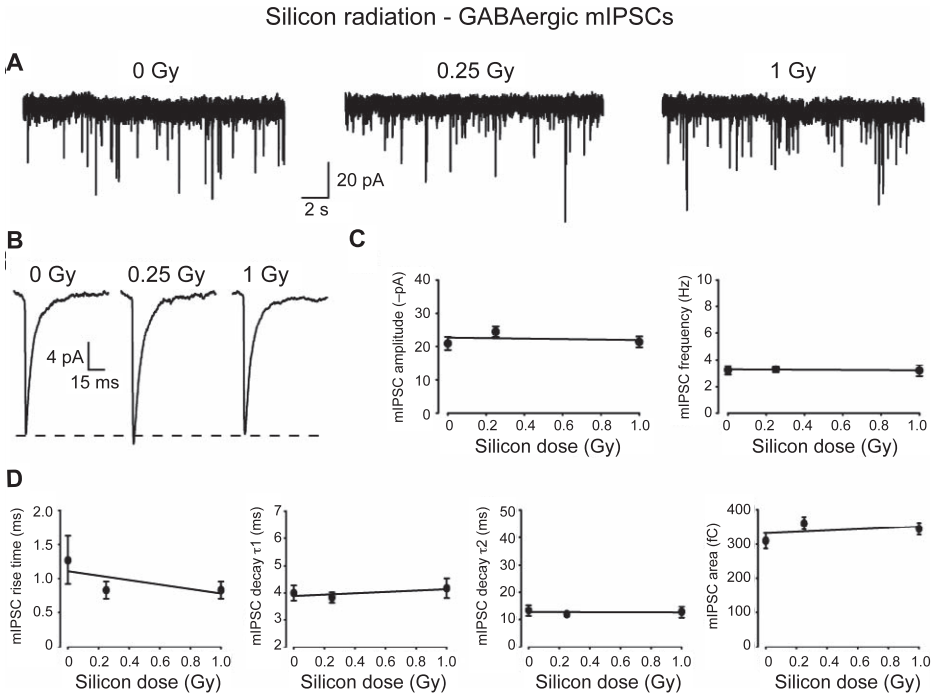

FIG. 4. Exposure to silicon radiation does not affect GABAergic synaptic transmission in the DG. Panel A: Representative current traces of mIPSCs recorded from DGCs of 0, 0.1, 0.5 and 1 Gy silicon-irradiated mice. Panel B: Average mIPSC traces of representative granule cells recorded from 0, 0.25 and 1 Gy silicon-irradiated mice. Panel C: Summary graphs showing that exposure to silicon radiation does not affect mIPSC amplitude and frequency in the DGCs (n = neurons/mice: 0 Gy, n = 16/3; 0.25 Gy, n = 19/5; 1 Gy, n = 19/5). Panel D: Summary graphs showing that mIPSC rise time, decay time (τ1 and τ2 constant) and area under the curve are not affected by exposure to silicon radiation.

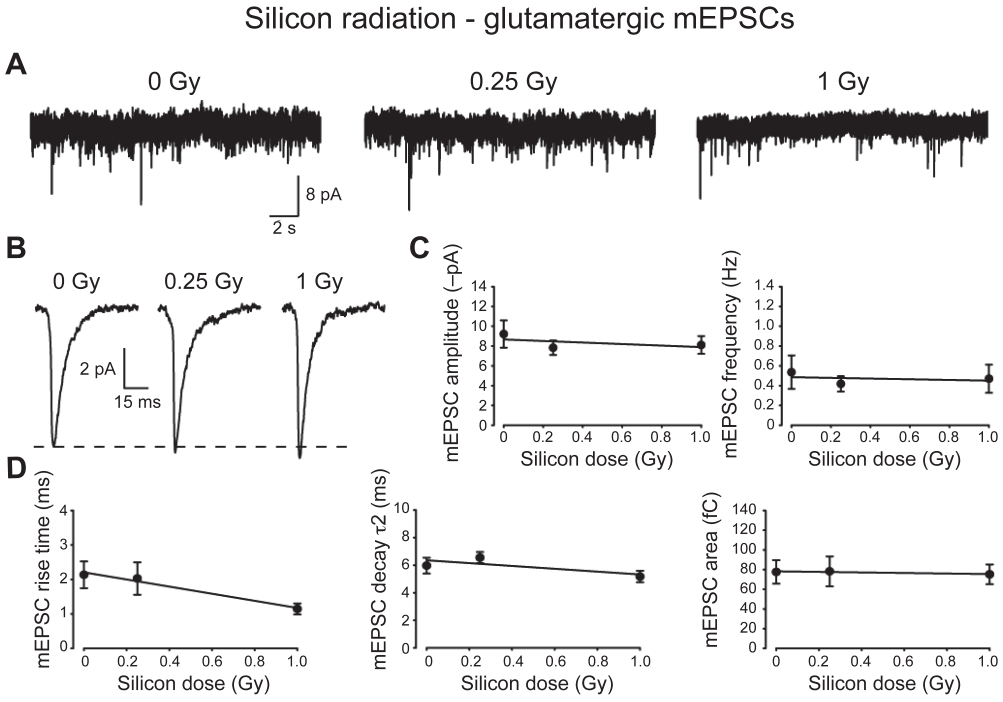

FIG. 5. Exposure to silicon radiation does not affect glutamatergic synaptic transmission in the DG. Panel A: Representative current traces of mEPSCs recorded from DGCs of 0, 0.25 and 1 Gy silicon-irradiated mice. Panel B: Average mEPSC traces of representative granule cells recorded from mice irradiated with 0, 0.25 and 1 Gy of silicon. Panel C: Summary graphs showing that silicon radiation does not affect mEPSC amplitude and frequency in the DGCs (n = neurons/mice: 0 Gy, n = 7/3; 0.25 Gy, n = 8/3; 1 Gy, n = 12/3). Panel D: Summary graphs showing that mEPSC rise time, decay time and area under the curve are not affected by silicon radiation.

TABLE 3
Effects of Silicon and Iron Radiation on mEPSC Parameters

Patch clamp radiation (no. of DGCs recorded)	mEPSC				
	Amplitude (pA)	Frequency (Hz)	Rise time (ms)	Decay τ1 (ms)	Area (fC)
Silicon					
0 Gy (7)	9.2 ± 1.4	0.5 ± 0.2	2.1 ± 0.4	5.2 ± 0.6	78 ± 12
0.25 Gy (8)	7.8 ± 0.7	0.4 ± 0.08	2.0 ± 0.5	5.4 ± 0.3	78 ± 15
1 Gy (6)	8.1 ± 0.9	0.5 ± 0.1	1.1 ± 0.2	4.3 ± 0.3	75 ± 10
Iron					
0 Gy (10)	8.4 ± 0.7	0.4 ± 0.05	1.1 ± 0.1	4.7 ± 0.3	77 ± 12
0.25 Gy (8)	7.3 ± 0.3	0.5 ± 0.1	1.1 ± 0.1	4.3 ± 0.3	91 ± 11
1 Gy (12)	9.0 ± 0.6	0.7 ± 0.1[a]	1.0 ± 0.1	4.5 ± 0.2	103 ± 9

Note. 0 Gy vs. 1 Gy.
[a] $P < 0.05$, one-way ANOVA.

0.05, Kruskal-Wallis one-way ANOVA on ranks), decay time ($P > 0.05$, Kruskal-Wallis one-way ANOVA on ranks) or area under the curve ($P > 0.05$, one-way ANOVA) (Fig. 5D and Table 3). Together, these data on GABAergic and glutamatergic synaptic transmission of DGCs are consistent with the lack of effect of silicon radiation on synaptic excitability and plasticity observed in extracellular recordings.

Iron Radiation Does Not Affect Synaptic Excitability in DGCs

Recordings obtained from DGCs of iron-irradiated mice were used to assess the effect of iron particle radiation on synaptic transmission in the DG. As expected, the input-output curve showed that incremental stimulation intensity significantly increases fEPSP peak-to-peak amplitude [$F(29,1247) = 140.1$, $^{***}P < 0.001$, two-way RM ANOVA] (Fig. 6). Iron radiation did not significantly affect the input-output outcomes [$F(2,1247) = 0.56$, $P > 0.05$, two-way RM ANOVA; stimulation intensity: 150 nA, fEPSP peak-to-peak amplitude: 0 Gy: 1,570 ± 200 μV, n = 17; 0.25 Gy: 1,643 ± 259 μV, n = 15; 1 Gy: 1,303 ± 185 μV, n = 14; $P > 0.05$] (Fig. 6). These results suggest that iron radiation does not affect the synaptic excitability of DGCs.

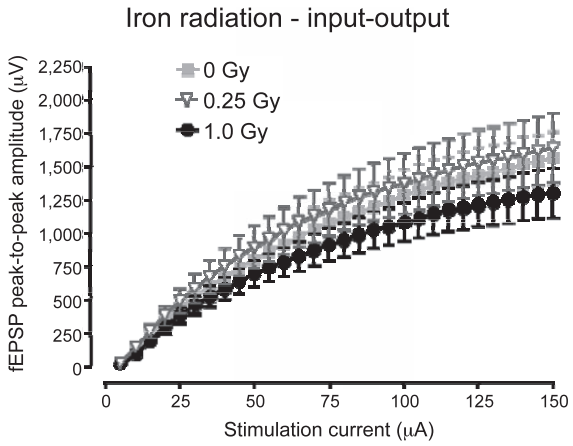

FIG. 6. Exposure to iron radiation does not modify synaptic excitability in the DG. Summary of input-output relationship showing that iron radiation does not modify the synaptic excitability of DGCs (n = slices/mice: 0 Gy, n = 17/11; 0.25 Gy, n = 15/11; 1 Gy, n = 14/10).

Iron Radiation Does Not Affect GABAergic, but Modifies Glutamatergic Synaptic Transmission in DGCs

To identify the effects of iron radiation on inhibitory and excitatory synaptic transmission, mIPSCs or mEPSCs were recorded from DGCs of 0, 0.25 and 1 Gy irradiated mice (Fig. 7A). Iron radiation produced no significant changes in mIPSC parameters (Fig. 7C, D). We observed a small trend to increased mIPSC amplitude ($P > 0.05$, one-way ANOVA), but no discernible trends for mIPSC frequency ($P > 0.05$, one-way ANOVA) (Fig. 7C and Table 2), rise time ($P > 0.05$, Kruskal-Wallis one-way ANOVA on ranks), decay time (τ_1, $P > 0.05$, one-way ANOVA; τ_2, $P > 0.05$, Kruskal-Wallis one-way ANOVA on ranks) or area under the curve ($P > 0.05$, one-way ANOVA) (Fig. 7D and Table 2).

In contrast, we observed that exposure to iron radiation did produce significant changes in mEPSCs of DGCs. Exposure to 1 Gy iron radiation significantly increased AMPAR mEPSCs frequency (0 vs. 1 Gy, $^{*}P < 0.05$, one-way ANOVA with Bonferroni post hoc test) without affecting mEPSC amplitude ($P > 0.05$, one-way ANOVA) (Fig. 8C and Table 3). In addition, mEPSC rise time ($P > 0.05$, one-way ANOVA), decay time ($P > 0.05$, one-way ANOVA) and area ($P > 0.05$, one-way ANOVA) were not significantly altered (Fig. 8D). These results suggest that iron radiation may potentiate glutamatergic synaptic transmission in DGCs through presynaptic increases in the vesicular release probability of glutamate.

DISCUSSION

The assessment of potential health risks associated with exposure to proton and HZE particle radiation is important for future long duration space missions. Here we demon-

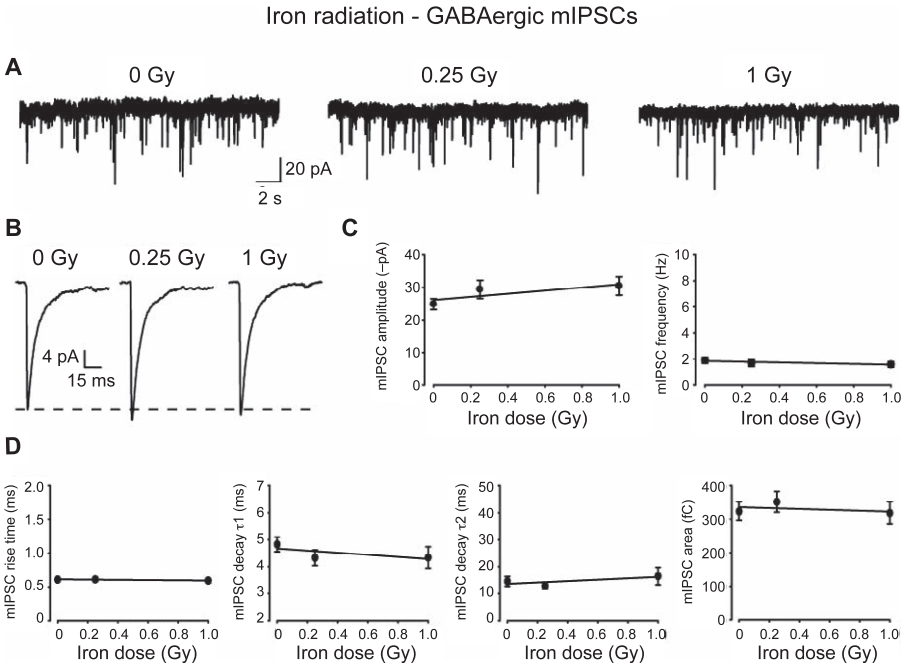

FIG. 7. Exposure to iron radiation does not affect GABAergic synaptic transmission in the DG. Panel A: Representative current traces of mIPSCs recorded from DGCs of 0, 0.25 and 1 Gy iron-irradiated mice. Panel B: Average mIPSC traces of representative DGCs recorded from 0, 0.25 and 1 Gy iron-irradiated mice. Panel C: Summary graphs showing that iron radiation does not affect mIPSC amplitude and frequency in the DGCs (n = neurons/mice: 0 Gy, n = 15/4; 0.25 Gy, n = 13/4; 1 Gy, n = 14/4. Panel D: Summary graphs showing that mIPSC rise time, decay time (τ1 and τ2 constant) and area under the curve are not affected by iron radiation.

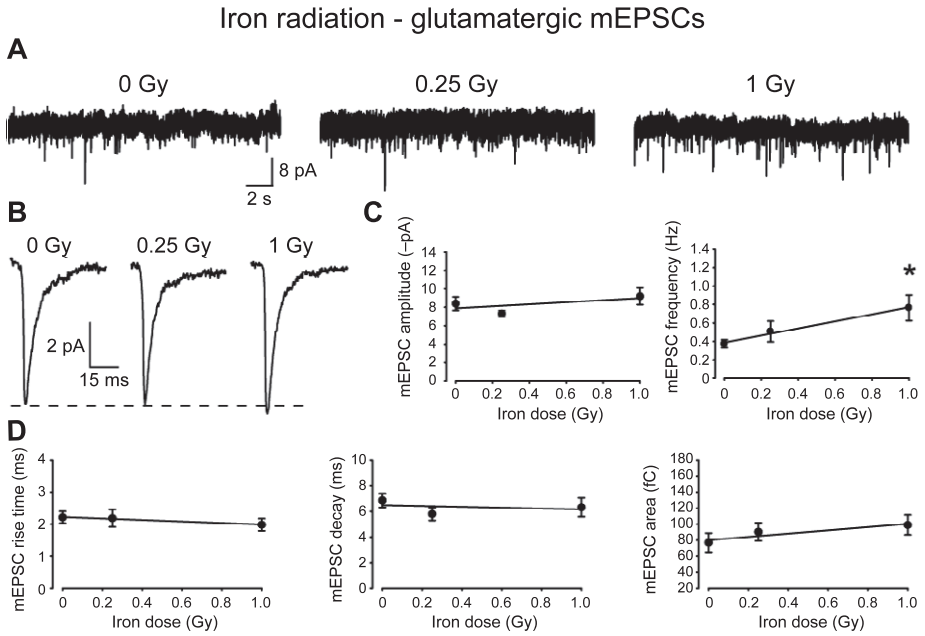

FIG. 8. Exposure to iron radiation modifies glutamatergic synaptic transmission in the DG. Panel A: Representative current traces of mEPSCs recorded from DGCs of 0, 0.25 and 1 Gy iron-irradiated mice. Panel B: Average mEPSC traces of representative granule cells recorded from 0, 0.25 and 1 Gy iron-irradiated mice. Panel C: Summary graphs showing the dose-dependent increase in mEPSC frequency in mice exposed to iron radiation (*$P < 0.05$), while mEPSC amplitude is unchanged (n = neurons/mice: 0 Gy, n = 10/4; 0.25 Gy, n = 8/4; 1 Gy, n = 12/4. Panel D: Summary graphs showing that mEPSC rise time, decay time and area under the curve are not affected by iron radiation.

strate that proton and HZE particle radiation have distinct effects on synaptic excitability and inhibitory synaptic transmission of DGCs in the dorsal hippocampus. We also show that iron radiation induces changes in excitatory synaptic transmission in the same cells. However, exposure to silicon radiation did not modify synaptic excitability or excitatory and inhibitory neurotransmission of DGCs. This study is the first to describe the effects of silicon radiation in the DG neurons. Learning and memory in the mammalian brain have prominent electrophysiological manifestations in the DG of the hippocampus. Synapses in the DGCs exhibit LTP (*33*), a specific form of synaptic plasticity is believed to contribute to long-term memory formation (*24, 33–35*). Synaptic excitability plays a critical role in the expression of LTP in the hippocampus. It has been shown that the reduction in LTP of CA1 neurons was attributed to radiation-induced increases in excitability, placing synapses in a potentiated state such that high-frequency stimulation *in vitro* fails to produce further increases in fEPSP (*27*). Thus, radiation-induced cognitive impairments could be associated with electrophysiological alterations in synaptic excitability of DGCs. In this study, we observed that 1 Gy proton irradiation increased synaptic excitability of DGCs. These neuroadaptive changes induced by proton radiation could lead to a dysregulation in the processing and integration of information within the hippocampus, which could play a crucial role in space radiation-induced impairment of hippocampal-dependent cognitive functions.

A fine balance between the excitatory glutamatergic and inhibitory GABAergic transmission in the DG is critical for proper operation of neuronal networks and cognitive health (*21–26*). It has been shown that the GABAergic-mediated synaptic inhibition plays a critical role in the modulation of synaptic plasticity, such as LTP, in the DG compared with the CA1 region (*25, 36*). In our extracellular recordings, the fEPSP responses to electrical stimulation are a sum of activated postsynaptic excitatory glutamatergic receptors and inhibitory GABAergic conductances. Thus, decreases in GABAergic inhibition allow for increased synaptic excitability and promote LTP (*25*), whereas enhanced GABAergic inhibition can reduce synaptic excitability and completely prevent the induction of LTP (*25*). In this study, we observed that exposure to proton radiation alters GABAergic synaptic transmission of the DGCs. The decreases in mIPSC amplitude and charge transfer observed in the DGCs of proton-irradiated mice suggest that proton radiation decreases the function of synaptic $GABA_AR$s. The channel kinetics and pharmacological sensitivity of $GABA_AR$s are largely dictated by their subunit composition and phosphorylation/dephosphorylation states (*29, 30, 37*). For example, we have previously demonstrated that altered expression and cellular localization of individual $GABA_AR$ subunits greatly affects postsynaptic $GABA_AR$ function of DGCs (*38*). It has also been shown that decreased synaptic clustering and expression of postsynaptic $GABA_AR$s produced decreases in mIPSC amplitude (*39*). However, in this current study we found that the expression of $GABA_AR$ subunits $\alpha2$, $\beta3$ and $\gamma2$, common to DGC inhibitory synapses (*31, 32*), was not modified in proton-irradiated mice suggesting that the decreased synaptic $GABA_AR$ function was likely due to alterations in their phosphorylation state or decreased synaptic clustering. This decrease in GABAergic synaptic inhibition may represent a cellular mechanism underlying proton radiation-induced increases in synaptic excitability of DGCs.

The effects of low-dose silicon radiation on cognitive functions and hippocampal synaptic neurotransmission are still unclear. Recent studies have shown that low doses of silicon radiation increase synaptic plasticity in the CA1 region of the hippocampus in naïve mice, and even further in cognitively tested mice (*14, 40*). In this current study, we found that exposure to silicon radiation has no effects on synaptic excitability, GABAergic or glutamatergic synaptic transmission of DGCs. These data suggest that the effects of low-dose silicon radiation on hippocampal neurotransmission and consequently on cognitive function may be selective for specific regions of the hippocampal formation.

It has been shown that relatively high doses of iron radiation (1–4 Gy) increase synaptic excitability and reduce LTP in CA1 pyramidal neurons of the hippocampus (*27*). Compared to DGCs, CA1 neurons are generally more excitable, have a weaker tonic inhibitory GABAergic drive and in slice recordings exhibit more depolarized membrane potentials. In this study, we showed that exposure to iron radiation does not significantly alter the synaptic excitability of DGCs. These results suggest that low-dose iron radiation can have different effects on synaptic properties in different regions of the hippocampus.

A previous study has demonstrated that low doses (0.6 Gy) of iron radiation induced a persistent reduction in glutamatergic readily releasable pool in hippocampal presynaptic terminals, suggesting that exposure to iron radiation may decrease the glutamate release probability in the hippocampus (*41*). In contrast, we found that exposure to iron radiation produces a dose-dependent increase in frequency of mEPSCs in DG granule cells suggestive of increased presynaptic glutamate release. This increase in mEPSC frequency suggests that the effects of iron radiation in the DG may be mediated by presynaptic increases in the probability of glutamate release (*42, 43*). However, this increase in presynaptic glutamate release probability was not paralleled by increases in evoked synaptic excitability in the DG granule cells in our extracellular I-O recordings (Fig. 6), nor in modifications in GABAergic mIPSCs (Fig. 7), nor in paired-pulse stimulation responses (see Materials and Methods; data not shown) that indirectly test for changes in presynaptic glutamate release. Therefore, since extracellular recordings demonstrated that fEPSPs were preferentially evoked by stimulation of the mPP axons, it is possible that the increased frequency of mEPSCs in intracellular measurements originated from synapses of other input pathways such as the commissural fibers.

Moreover, all mEPSC recordings were performed during blockade of $GABA_A$ and $GABA_B$ receptor blockers, as opposed to fEPSP recordings where modulatory effects of GABAergic interneuron activation may have precluded detection of changes in fEPSPs evoked by intense presynaptic stimulation. Thus, our study suggests that modification of the glutamatergic synaptic transmission, rather than alteration of GABAergic inhibition and synaptic excitability in the DG as shown with proton irradiation, may cause the impairment of hippocampal-dependent cognitive functions induced by exposure to iron radiation. Recent studies have shown that low-dose iron radiation induces a persistent deficit in hippocampal-dependent cognitive functions, including spatial learning (*5*) and contextual freezing, which was correlated to the number of neurons expressing the protein Arc, a plasticity-related protein essential for memory consolidation (*44*), in the enclosed (bottom) and free (upper) blade of the DG (*6*). Our current extracellular and whole cell patch-clamp recordings have not addressed possible differences in the electrophysiological properties and radiation responses of Arc-positive neurons, which may be a fruitful area for future investigations.

The molecular mechanisms by which particle radiation affects synaptic neurotransmission and cognitive performance are still unclear. The data presented in this study suggest that radiation-induced alterations in DG neurotransmission may be quite complex and involve mechanisms that need further investigation. Damage induced by ionizing radiation to living cells is directly related to the track structure of ionizing radiation in matter (*45, 46*). Insults from ionizing radiation take the form of highly structured tracks of ionized and excited molecules leading to the production of free radicals and reactive oxygen species (ROS) (*2, 3, 47, 48*) that are highly damaging to DNA, lipids and proteins in living cells (*49*). Poisson distribution calculations indicate that for neurons of nuclear area 60 μm^2 typical of hippocampal neurons (*50*), a 0.25 Gy dose of silicon radiation results in an average of 2.1 particle traversals per nucleus with 12% of cells untraversed ''unhit'' while a 1 Gy dose results in an average of 8.6 traversals per cell nucleus and with less than 0.02% of the cells remaining unhit. For iron radiation, a 0.25 Gy dose results in an average of 0.54 particle traversals per nucleus and 58% of cells remaining unhit, while a 1 Gy dose results in an average of 2.2 traversals per cell nucleus and 12% of cells being unhit. For protons, all doses $\geq$0.1 Gy result in at least 66 traversals per cell and essentially no unhit cells. Thus, it is likely that the differential effects of proton, silicon and iron radiations on DG synaptic neurotransmission could be related to the ability of their different track structures to effectively generate oxidative stress within the cells. Several studies have shown that ROS can regulate signaling pathways (*51*), modulate synaptic transmission (*52*) and plasticity in the hippocampus (*51, 53*). Therefore, the differential effects of ionized radiation on cellular ROS production could be responsible for the differential effects of proton, silicon and iron on synaptic transmission of DGCs. Overexpression of the mitochondrial-targeted human catalase (MCAT) transgene in mice, has been shown to decrease the overall production of free radicals, significantly reduced mitochondrial ROS and improved hippocampal neurogenesis after low-dose exposure to proton radiation (*54*). Examination of differences in synaptic neurotransmission and radiation responses of DGCs from MCAT mice would be useful to determine if their resistance to the harmful effects of low-dose radiation also extends to protection from radiation-induced changes in DG synaptic neurotransmission.

In conclusion, this study demonstrates that space radiation induces long-lasting neuroadaptive changes in the synaptic neurotransmission of the hippocampal DG network, which could represent the cellular and molecular mechanisms responsible for space radiation-induced hippocampal-dependent cognitive dysfunctions. Nevertheless, the relationship between radiation-induced cognitive impairment and synaptic neurotransmission is complex and needs to be carefully assessed within the context of a set of radiation exposures to better understand the mechanisms involved, and to develop innovative strategies to effectively protect astronauts against the detrimental effects of space radiation during long-term space exploration.

ACKNOWLEDGMENTS

This work was supported by National Aeronautics and Space Administration grant NNX10AD59G. We thank Dr. Werner Sieghart (Medical University of Vienna, Vienna, Austria) for the gift of the $GABA_AR$ subunit antibodies.

Received: December 19, 2013; accepted: August 22, 2014; published online: November 19, 2014

REFERENCES

1. Manda K, Ueno M, Anzai K. Space radiation-induced inhibition of neurogenesis in the hippocampal dentate gyrus and memory impairment in mice: ameliorative potential of the melatonin metabolite, AFMK. J Pineal Res 2008; 45:430–8.
2. Limoli CL, Giedzinski E, Baure J, Rola R, Fike JR. Redox changes induced in hippocampal precursor cells by heavy ion irradiation. Radiat Environ Biophys 2007; 46:167–72.
3. Giedzinski E, Rola R, Fike JR, Limoli CL. Efficient production of reactive oxygen species in neural precursor cells after exposure to 250 MeV protons. Radiat Res 2005; 164:540–4.
4. Cucinotta FA, Durante M. Cancer risk from exposure to galactic cosmic rays: implications for space exploration by human beings. Lancet Oncol 2006; 7:431–5.
5. Britten RA, Davis LK, Johnson AM, Keeney S, Siegel A, Sanford LD, et al. Low (20 cGy) doses of 1 GeV/u (56)Fe–particle radiation lead to a persistent reduction in the spatial learning ability of rats. Radiat Res 2012; 177:146–51.
6. Raber J, Allen AR, Rosi S, Sharma S, Dayger C, Davis MJ, et al. Effects of whole body (56)Fe radiation on contextual freezing and

Arc-positive cells in the dentate gyrus. Behav Brain Res 2013; 246:162–7.

7. Rola R, Zou Y, Huang TT, Fishman K, Baure J, Rosi S, et al. Lack of extracellular superoxide dismutase (EC-SOD) in the microenvironment impacts radiation-induced changes in neurogenesis. Free Radic Biol Med 2007; 42:1133–45; discussion 31–2.
8. Monje ML, Mizumatsu S, Fike JR, Palmer TD. Irradiation induces neural precursor-cell dysfunction. Nat Med 2002; 8:955–62.
9. Rola R, Raber J, Rizk A, Otsuka S, VandenBerg SR, Morhardt DR, et al. Radiation-induced impairment of hippocampal neurogenesis is associated with cognitive deficits in young mice. Exp Neurol 2004; 188:316–30.
10. Rola R, Otsuka S, Obenaus A, Nelson GA, Limoli CL, VandenBerg SR, et al. Indicators of hippocampal neurogenesis are altered by 56Fe-particle irradiation in a dose-dependent manner. Radiat Res 2004; 162:442–6.
11. Moravan MJ, Olschowka JA, Williams JP, O'Banion MK. Cranial irradiation leads to acute and persistent neuroinflammation with delayed increases in T-cell infiltration and CD11c expression in C57BL/6 mouse brain. Radiat Res 2011; 176:459–73.
12. Rosi S, Andres-Mach M, Fishman KM, Levy W, Ferguson RA, Fike JR. Cranial irradiation alters the behaviorally induced immediate-early gene arc (activity-regulated cytoskeleton-associated protein). Cancer Res 2008; 68:9763–70.
13. Raber J, Rosi S, Chakraborti A, Fishman K, Dayger C, Davis MJ, et al. Effects of (56)Fe-particle cranial radiation on hippocampus-dependent cognition depend on the salience of the environmental stimuli. Radiat Res 2011; 176:521–6.
14. Raber J, Rola R, LeFevour A, Morhardt D, Curley J, Mizumatsu S, et al. Radiation-induced cognitive impairments are associated with changes in indicators of hippocampal neurogenesis. Radiat Res 2004; 162:39–47.
15. Jaffe DB, Gutierrez R. Mossy fiber synaptic transmission: communication from the dentate gyrus to area CA3. Prog Brain Res 2007; 163:109–32.
16. Kesner RP. Behavioral functions of the CA3 subregion of the hippocampus. Learn Mem 2007; 14:771–81.
17. Aimone JB, Deng W, Gage FH. Resolving new memories: a critical look at the dentate gyrus, adult neurogenesis, and pattern separation. Neuron 2011; 70:589–96.
18. Deng W, Aimone JB, Gage FH. New neurons and new memories: how does adult hippocampal neurogenesis affect learning and memory? Nat Rev Neurosci 2011; 11:339–50.
19. Inokuchi K. Adult neurogenesis and modulation of neural circuit function. Curr Opin Neurobiol 2011; 21:360–4.
20. Rola R, Sarkissian V, Obenaus A, Nelson GA, Otsuka S, Limoli CL, et al. High-LET radiation induces inflammation and persistent changes in markers of hippocampal neurogenesis. Radiat Res 2005; 164:556–60.
21. Gibbs ME, Johnston GA. Opposing roles for GABAA and GABAC receptors in short-term memory formation in young chicks. Neuroscience 2005; 131:567–76.
22. Hara Y, Punsoni M, Yuk F, Park CS, Janssen WG, Rapp PR, et al. Synaptic distributions of GluA2 and PKMzeta in the monkey dentate gyrus and their relationships with aging and memory. J Neurosci 2012; 32:7336–44.
23. Tamminga CA, Southcott S, Sacco C, Wagner AD, Ghose S. Glutamate dysfunction in hippocampus: relevance of dentate gyrus and CA3 signaling. Schizophr Bull 2012.
24. Richter-Levin G, Canevari L, Bliss TV. Long-term potentiation and glutamate release in the dentate gyrus: links to spatial learning. Behav Brain Res 1995; 66:37–40.
25. Arima-Yoshida F, Watabe AM, Manabe T. The mechanisms of the strong inhibitory modulation of long-term potentiation in the rat dentate gyrus. Eur J Neurosci 2011; 33:1637–46.
26. Morellini F, Sivukhina E, Stoenica L, Oulianova E, Bukalo O, Jakovcevski I, et al. Improved reversal learning and working memory and enhanced reactivity to novelty in mice with enhanced GABAergic innervation in the dentate gyrus. Cereb Cortex 2010; 20:2712–27.
27. Vlkolinsky R, Krucker T, Smith AL, Lamp TC, Nelson GA, Obenaus A. Effects of lipopolysaccharide on 56Fe-particle radiation-induced impairment of synaptic plasticity in the mouse hippocampus. Radiat Res 2007; 168:462–70.
28. Gilbert ME, Burdette LJ. Hippocampal field potential: A model system to characterize neurotoxicology. In: L. W. Chang and W. Slikker J, editor. Neurotoxicology: approaches and methods. Waltham, MA: Academic Press; 1995. p. 183–203.
29. Houston CM, He Q, Smart TG. CaMKII phosphorylation of the GABA(A) receptor: receptor subtype- and synapse-specific modulation. J Physiol 2009; 587:2115–25.
30. Olsen RW, Sieghart W. International Union of Pharmacology. LXX. Subtypes of gamma-aminobutyric acid(A) receptors: classification on the basis of subunit composition, pharmacology, and function. Update. Pharmacol Rev 2008; 60:243–60.
31. Herd MB, Haythornthwaite AR, Rosahl TW, Wafford KA, Homanics GE, Lambert JJ, et al. The expression of GABAA beta subunit isoforms in synaptic and extrasynaptic receptor populations of mouse dentate gyrus granule cells. J Physiol 2008; 586:989–1004.
32. Suryanarayanan A, Liang J, Meyer EM, Lindemeyer AK, Chandra D, Homanics GE, et al. Subunit compensation and plasticity of synaptic GABA(A) receptors induced by ethanol in alpha4 subunit knockout mice. Front Neurosci 2011; 5:110.
33. Abraham WC, Williams JM. Properties and mechanisms of LTP maintenance. Neuroscientist 2003; 9:463–74.
34. Malenka RC, Nicoll RA. Learning and memory. Never fear, LTP is hear. Nature 1997; 390:552–3.
35. Maren S, Baudry M. Properties and mechanisms of long-term synaptic plasticity in the mammalian brain: relationships to learning and memory. Neurobiol Learn Mem 1995; 63:1–18.
36. Wigstrom H, Gustafsson B. Facilitated induction of hippocampal long-lasting potentiation during blockade of inhibition. Nature 1983; 301:603–4.
37. Vithlani M, Moss SJ. The role of GABAAR phosphorylation in the construction of inhibitory synapses and the efficacy of neuronal inhibition. Biochem Soc Trans 2009; 37:1355–8.
38. Liang J, Suryanarayanan A, Abriam A, Snyder B, Olsen RW, Spigelman I. Mechanisms of reversible GABAA receptor plasticity after ethanol intoxication. J Neurosci 2007; 27:12367–77.
39. Kilman V, van Rossum MC, Turrigiano GG. Activity deprivation reduces miniature IPSC amplitude by decreasing the number of postsynaptic GABA(A) receptors clustered at neocortical synapses. J Neurosci 2002; 22:1328–37.
40. Rudobeck E, Nelson GA, Sokolova IV, Vlkolinsky R. Silicon radiation impairs neuronal output in CA1 neurons of mouse ventral hippocampus without altering dendritic excitability. Radiat Res 2014; 181:407–15.
41. Machida M, Lonart G, Britten RA. Low (60 cGy) doses of (56)Fe HZE-particle radiation lead to a persistent reduction in the glutamatergic readily releasable pool in rat hippocampal synaptosomes. Radiat Res 2010; 174:618–23.
42. Korn H, Triller A, Mallet A, Faber DS. Fluctuating responses at a central synapse: n of binomial fit predicts number of stained presynaptic boutons. Science 1981; 213:898–901.
43. Del Castillo J, Katz B. Quantal components of the end-plate potential. J Physiol 1954; 124:560–73.
44. Plath N, Ohana O, Dammermann B, Errington ML, Schmitz D, Gross C, et al. Arc/Arg3.1 is essential for the consolidation of synaptic plasticity and memories. Neuron 2006; 52:437–44.
45. Plante I, Ponomarev AL, Cucinotta FA. Calculation of the energy deposition in nanovolumes by protons and HZE particles: geometric patterns of initial distributions of DNA repair foci. Phys Med Biol 2013; 58:6393–405.

46. George KA, Hada M, Chappell L, Cucinotta FA. Biological effectiveness of accelerated particles for the induction of chromosome damage: track structure effects. Radiat Res 2013; 180:25–33.

47. Sun J, Chen Y, Li M, Ge Z. Role of antioxidant enzymes on ionizing radiation resistance. Free Radic Biol Med 1998; 24:586–93.

48. Denisova NA, Shukitt-Hale B, Rabin BM, Joseph JA. Brain signaling and behavioral responses induced by exposure to (56)Fe-particle radiation. Radiat Res 2002; 158:725–34.

49. Manda K, Ueno M, Anzai K. Memory impairment, oxidative damage and apoptosis induced by space radiation: ameliorative potential of alpha-lipoic acid. Behav Brain Res 2008; 187:387–95.

50. Curtis SB, Vazquez ME, Wilson JW, Atwell W, Kim MH. Cosmic ray hits in the central nervous system at solar maximum. Adv Space Res 2000; 25:2035–40.

51. Klann E, Thiels E. Modulation of protein kinases and protein phosphatases by reactive oxygen species: implications for hippocampal synaptic plasticity. Prog Neuropsychopharmacol Biol Psychiatry 1999; 23:359–76.

52. Pellmar TC. Peroxide alters neuronal excitability in the CA1 region of guinea-pig hippocampus in vitro. Neuroscience 1987; 23:447–56.

53. Auerbach JM, Segal M. Peroxide modulation of slow onset potentiation in rat hippocampus. J Neurosci 1997; 17:8695–701.

54. Liao AC, Craver BM, Tseng BP, Tran KK, Parihar VK, Acharya MM, et al. Mitochondrial-targeted human catalase affords neuroprotection from proton irradiation. Radiat Res 2013.